Extratropical Transition of Tropical Cyclones over the Western North Pacific. Part II: The Impact of Midlatitude Circulation Characteristics

PATRICK A. HARR AND RUSSELL L. ELSBERRY

Department of Meteorology, Naval Postgraduate School, Monterey, California

TIMOTHY F. HOGAN

Naval Research Laboratory–Monterey, Monterey, California

(Manuscript received 18 January 1999, in final form 7 December 1999)

ABSTRACT

Two characteristic midlatitude circulation patterns (labeled northwest and northeast) are found to be associated with extratropical transition (ET) of tropical cyclones over the western North Pacific Ocean. Although in both cases the tropical cyclone moves poleward ahead of a midlatitude trough, the primary midlatitude circulation is either that trough or is a large quasi-stationary cyclone to the northeast of the poleward-moving tropical cyclone. Transition into a northwest pattern typically results in the development within 36 h of an intense extratropical cyclone that moves north–northeast. A tropical cyclone that moves into a northeast pattern enters into strong zonal flow between the primary midlatitude circulation and the subtropical ridge to the southeast. These systems move rapidly eastward and do not intensify significantly during the 36 h following transition.

In Part I of this study, the ET of Typhoon (TY) David (1997) and the ET of TY Opal (1997) were investigated in terms of the formation of extratropical cyclone features. In this study, the same cases of ET are examined to define interactions between the decaying tropical cyclone and these two general synoptic environments in terms of the distributions of heat and momentum fluxes and generation of kinetic energy between the cyclone and the environment. During transition into either circulation pattern, the tropical cyclone is initially impacted by upper-tropospheric eddy angular momentum fluxes associated with the juxtaposition of the midlatitude circulation. During transition into a northwest pattern, the tropical cyclone couples with the midlatitude baroclinic zone such that low-level eddy heat fluxes contribute to the extratropical cyclone development. During transition into a northeast pattern, the strong zonal flow seems to prevent a direct interaction between the decaying tropical cyclone and the primary midlatitude circulation. Eddy heat fluxes do not increase and minimal baroclinic development occurs.

The two types of extratropical transition also have significant differences in the generation of kinetic energy during the reintensification as an extratropical cyclone. Extratropical transition into a northwest pattern results in barotropic and baroclinic production of kinetic energy through direct solenoidal circulations that result from the coupling of the tropical cyclone and midlatitude trough. The movement of a tropical cyclone toward the large, quasi-stationary extratropical cyclone in the northeast pattern results in barotropic destruction of kinetic energy that inhibits significant reintensification.

1. Introduction

As a tropical cyclone (TC) begins to recurve into the midlatitude westerlies, the characteristic TC structure changes in response to gradients of atmospheric wind (including vertical shear), temperature, and moisture. Often, the structural changes lead to the transition of the TC into an extratropical cyclone. Klein et al. (2000) define a conceptual model of extratropical transition (ET) as a two-stage process that consists of a *transformation* of the TC structural characteristics and then a *reintensification* as an extratropical cyclone. Through examination of 30 ET cases over the western North Pacific, Klein et al. (2000) showed that the transformation stage of the ET process proceeded through three steps in a similar manner for all cases studied. The basic physical characteristics of the transformation stage, which are identifiable in satellite imagery, are the asymmetric patterns of cloud and precipitation due to environmental inflow of colder, drier (warm, moist) air in the western (eastern) portion of the outer TC circulation. The reintensification stage is dominated by the evolution of extratropical cyclone features such as fronts and asymmetric wind, cloud, and precipitation patterns. Both stages of the transition of a TC into an extratropical cyclone involve many complex physical processes (Pal-

Corresponding author address: Patrick A. Harr, Code MR/Hp, Department of Meteorology, Root Hall, 589 Dyer Rd., Monterey, CA 93943-5114.
E-mail: paharr@nps.navy.mil

men 1958; DiMego and Bosart 1982a,b; Anthes 1990; Sinclair 1993; Browning et al. 1998).

This study and a companion study (Harr and Elsberry 2000) address how the reintensification of the decaying TC as an extratropical cyclone is affected by the character of the midlatitude circulation into which the decaying TC moves. In the Harr and Elsberry (2000) study, frontogenesis was used as a proxy for the change from a TC structure to an asymmetric extratropical cyclone structure. In this part, it will be shown that the midlatitude circulation impacts the exchange of heat and momentum between the midlatitudes and TC, and the generation of kinetic energy during the reintensification stage of ET.

Klein et al. (2000) show the change in structural characteristics during the transformation stage of ET is due to the movement of the TC into the midlatitude environment. Similarly, the formation of frontal regions during the *initial* steps of reintensification is dominated by the interaction between the TC and the midlatitude baroclinic zone and is relatively independent of the midlatitude circulation pattern. However, Harr and Elsberry (1999) found that the *final* structural characteristics of the reintensifying extratropical cyclone differ greatly depending on the character of midlatitude circulation into which the TC moves. In a *northwest* pattern, the coupling of the TC remnants with the eastward-moving midlatitude trough located northwest of the TC is so vigorous that an intense extratropical cyclone with well-defined frontal characteristics forms to become the primary circulation over the region. A weaker trough exists upstream in the *northeast* pattern, which is dominated by a preexisting, quasi-stationary extratropical cyclone northeast of the TC. In this case, the coupling between the midlatitude trough and the TC is reduced due to the influence of the preexisting midlatitude cyclone, and only weak warm frontogenesis occurs to the northeast of the reintensifying TC.

Various research groups have examined the influence of a midlatitude trough on the intensity change of the TC. An upstream upper-level trough, which may be characterized as a potential vorticity (PV) maximum, may intensify the TC through eddy fluxes of angular momentum (Molinari and Vollaro 1989, 1990) and potential vorticity (Molinari et al. 1995, 1998). However, these (and other) studies suggest other internal mechanisms (i.e., enhanced air–sea fluxes, initiation of an eyewall replacement cycle) may contribute during the intensification of a TC. Similarly, other aspects of the midlatitude environment such as decreasing sea surface temperature, increasing vertical wind shear, and the import of eddy fluxes to the TC, may contribute to the ET of a TC. A framework for the environmental interaction during ET is provided by generalized relationships between large-scale midlatitude circulations and the structure of individual cyclones that have been studied in some detail (Davies et al. 1991; Whitaker and Barcilon 1992; Thorncroft et al. 1993; Evans et al. 1994; Schultz et al. 1998).

In this study, the northwest and northeast circulation patterns are generalized in section 3 based on composite circulation patterns from 30 ET cases over the western North Pacific. Using the cases of Typhoon (TY) David (September 1997) and TY Opal (June 1997) as examples, the role of each midlatitude circulation is then examined more fully in terms of the heat and momentum fluxes (section 4) and the budget of kinetic energy (section 5) during reintensification. The diagnostic framework used in section 4 to compare the effect of environmental sources of PV on a *decaying* TC is similar to that used by Molinari et al. (1995) to diagnose the interactions leading to *intensification* of Hurricane Elena in the Gulf of Mexico during August 1985. Although both the David and Opal cases have large upper-level eddy angular momentum fluxes toward the TC as it moves into the midlatitudes, a significant difference is found due to eddy heat fluxes at lower levels that affect the baroclinic energy conversions.

Previous studies of the kinetic energy budget associated with the ET of tropical cyclones over the North Atlantic (Palmen 1958; Vincent and Chang 1975; Kornegay and Vincent 1976; Chien and Smith 1977; DiMego and Bosart 1982b) have varying results that may be due to different environments around the transforming TC. The kinetic energy budgets associated with the reintensification stage of TY Opal and TY David over the western North Pacific are examined in section 5 and interpreted with respect to the influence of each midlatitude circulation pattern.

2. Data

During June–October 1994–98, 30 cases of extratropical transition over the western North Pacific occurred (Table 1 in Klein et al. 2000). Environmental fields analyzed by the Naval Operational Global Atmospheric Prediction System (NOGAPS) at the Fleet Numerical Meteorology and Oceanography Center (Hogan and Rosmond 1991) are used to define the midlatitude circulation and calculate the various diagnostic quantities that will be used to examine the interactions between the TC and midlatitude environment. One benefit of the NOGAPS fields is the operational use of satellite water vapor winds that provide an additional data source, particularly in cloud-free regions of the middle and upper troposphere where this investigation into the interactions between the TC and midlatitudes is based.

Although no formal definition exists for specifying when ET has occurred, Harr and Elsberry (2000) propose use of a frontogenesis parameter to define the time of ET. Application of their definition is complicated by a change in the grid resolution of the NOGAPS analysis that occurred between 1994 and 1998. Consequently, the transition time and location were chosen based on

a more operationally oriented measure defined as the first synoptic time (i.e., 0000 or 1200 UTC) after the last operational TC warning issued by the Joint Typhoon Warning Center, Guam. For the cases of TY David and TY Opal analyzed by Harr and Elsberry (2000), these two ET definitions were identical. For each of the 30 ET cases, analyzed 500-hPa heights and sea level pressure at the ET time were defined on a grid with 1° lat–long resolution over a domain of 17° lat and 25° long such that the position of the transforming TC was located at 7° lat and 13° long from the lower-left corner of the grid. Composites were then constructed based on an empirical orthogonal function (EOF) analysis (Richman 1986) to define two characteristic circulation patterns associated with each case of ET over the western North Pacific.

The kinetic energy budgets associated with the ET cases of TY David and TY Opal are computed on isobaric surfaces using a 1° lat–long grid at all mandatory levels from 1000 to 100 hPa. The influence of the environment on the TC in terms of the exchange of heat and momentum is determined in a quasigeostrophic framework using Eliassen–Palm (EP) fluxes (Eliassen and Palm 1961). It has been shown (Edmon et al. 1980) that the divergence of the EP flux is directly proportional to the radial quasigeostrophic PV flux. To aid in this interpretation and to be consistent with the analysis of Molinari et al. (1995), the EP analysis is performed in isentropic coordinates at 5 K intervals from 305 to 405 K. The choice of 305 K as the lowest level was to avoid situations in which the isentropic surface intersected the ground, and the 405 K level was chosen since it represented the lower stratosphere. The basic synoptic environment during the two cases is defined by hydrostatic Ertel PV defined on each isentropic surface by

$$\Pi = -g(\zeta_\theta + f)/(\partial p/\partial \theta),$$

where the θ subscript indicates that the relative vorticity $\zeta\theta$ is evaluated on isentropic surfaces. Vertical and horizontal derivatives were computed with centered differences.

3. Midlatitude circulation characteristics

To provide a general context for the large-scale circulation influences on ET, two characteristic circulation patterns were defined objectively from the EOF patterns of the 30 ET cases during June–October 1994–98. Each case was then classified according to which circulation pattern was dominant at the time of ET. Composite 500-hPa and sea level pressure patterns (Fig. 1) were constructed that illustrate the circulation pattern at the time of ET and 24 h after the ET time. As in Harr and Elsberry (1999), physical meaning was attached to the location of the primary midlatitude circulation feature with respect to the decaying TC. The northwest pattern (Figs. 1a,b), which was based on 13 cases, was defined such that ET occurred downstream of a midlatitude trough. That is, the lowest 500-hPa heights and associated sea level pressure cyclone were northwest of the TC center. In the 24 h following the assigned ET time, the sea level pressure cyclone in these northwest cases followed a track to the north–northeast (Fig. 1b). As illustrated in Fig. 2a, other cyclones in the northwest circulation pattern tended to move poleward in the steering flow between the midlatitude cyclone to the northwest and strong ridge to the east. For the 17 cases in the northeast pattern (Figs. 1c,d), the midlatitude trough west of the decaying TC was weak and the midlatitude circulation was dominated by a large quasi-stationary cyclone at 500 hPa and at sea level that was northeast of the TC center. Notice the decaying TC in the northeast pattern was immediately west of a strong height gradient between the midlatitude cyclone to the northeast and the flattened subtropical ridge to the southeast. During the 24 h following the ET time, the decaying TC typically moved eastward due to the strong zonal flow between these two synoptic features while remaining as a distinct secondary low to the primary midlatitude circulation. Other cyclones in the northeast pattern (Fig. 2b) also moved in a zonal direction.

These two circulation patterns represented by the composites of ET cases are consistent with basic large-scale flow patterns associated with midlatitude cyclone development as classified by Evans et al. (1994). Schultz et al. (1998) and Sinclair and Revell (2000) have broadly categorized the large-scale flow patterns associated with midlatitude cyclone development as consisting of either diffluent (similar to the northwest pattern) or confluent (similar to the northeast pattern) background flow.

Klein et al. (2000) examined the variability of several physical characteristics associated with ET into the northwest and northeast circulation patterns. During the *transformation* stage of ET, there were no significant differences in terms of size (km) or intensity (kt) between cases that undergo ET into a northwest or northeast pattern. However, there was a statistically significant difference in sea level pressure during *reintensification* associated with the circulation pattern into which the decaying TC moves. The mean sea level pressure after 36 h into the reintensification phase of ET in a northwest pattern was 978 hPa with a standard deviation of 9 hPa, while the mean sea level pressure in a northeast pattern was 991 hPa with a standard deviation of 12 hPa.

4. Influence on extratropical transition

In this section, the influences of the midlatitude circulation pattern on the decaying TC during the reintensification stage of ET in the two characteristic circulations are examined. The synoptic analyses for TY David (a northwest pattern case) and TY Opal (a northeast case) are presented in Harr and Elsberry (2000). Molinari et al. (1995) studied the interaction of Hurricane Elena with an upper-level trough (i.e., upper-level PV

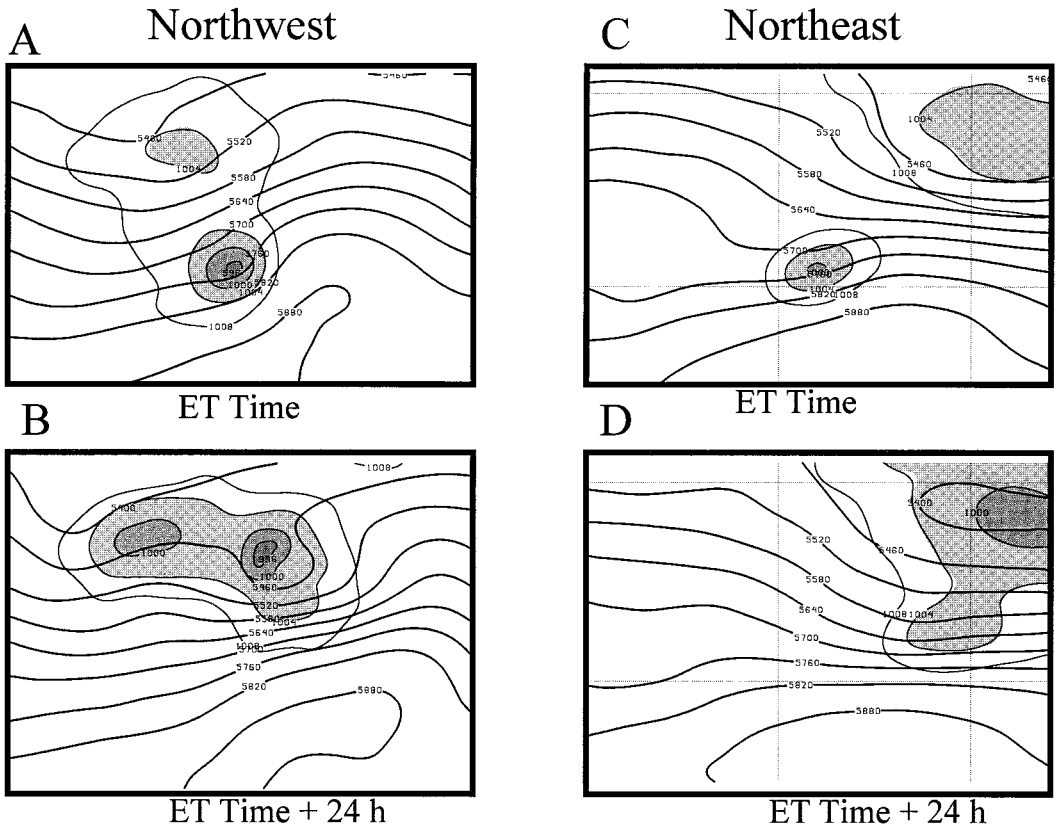

FIG. 1. Composite 500-hPa height (m) and sea level pressure (hPa, only below 1008 hPa with shading in 4-hPa increments starting at 1004 hPa) analyses based on grouping of cases in a northwest pattern at the (a) ET time, (b) ET + 24 h, and in a northeast pattern at the (c) ET time and (d) ET + 24 h. The composite northwest pattern is based on 13 cases and the northeast pattern is based in 17 cases.

maximum) approaching from the west, which would be classified as a northwest pattern. They concluded that the outflow from a mature TC that is still over warm water with strong deep convection throughout the inner core may reinforce the upper-level anticyclone. If the resulting distortion of the approaching PV anomaly then reduces the dynamic scale of the upper-level PV distribution, a favorable interaction may occur (i.e, preventing the disruption of the warm core by vertical shear) that results in intensification of the TC.

Although Molinari et al. (1995) do not directly address extratropical transition, they suggest that a TC over cooler waters may not be able to maintain deep inner-core convection, which would not allow the upper-level anticyclone to reduce the scale of an approaching upper-level trough. Less resistance to the differential effects of vertical shear may then diminish the warm core aloft. Using the relationship between the EP flux divergence and eddy PV flux (Edmon et al. 1980), Molinari et al. (1995) showed that positive PV anomalies were brought into a cylinder around the hurricane, while negative PV anomalies were removed. In the case of the intensifying Hurricane Elena, barotropic processes were most important as the maximum EP flux vectors were dominated by eddy angular momentum fluxes at one level (345 K). Therefore, it is of interest to compare these results with the relative roles of both eddy momentum and heat fluxes during extratropical transition and baroclinic redevelopment.

Synoptic distributions of PV on isentropic surfaces have been examined for each case over a 48-h period that contains the reintensification of the decaying TC as an extratropical cyclone. The influence of the environmental PV distribution on the TC circulation was diagnosed using EP fluxes as in Molinari et al. (1995) with a storm-following cylindrical coordinate system. As detailed derivations of the EP flux equations are available in Andrews (1983) and Molinari et al. (1995), only a summary is presented here. The storm-relative radial velocity u is defined positive outward and the tangential velocity v is defined positive counterclockwise. A pseudodensity is defined as $\sigma = -\partial p/\partial\theta$ and the Montgomery streamfunction is defined as $M = c_pT + gz$, where T is the temperature, c_p is the specific heat of air at constant pressure, and z is the geometric height.

The EP framework is based on the relationship between the time change in relative angular momentum (i.e., pseudodensity-weighted tangential wind multiplied

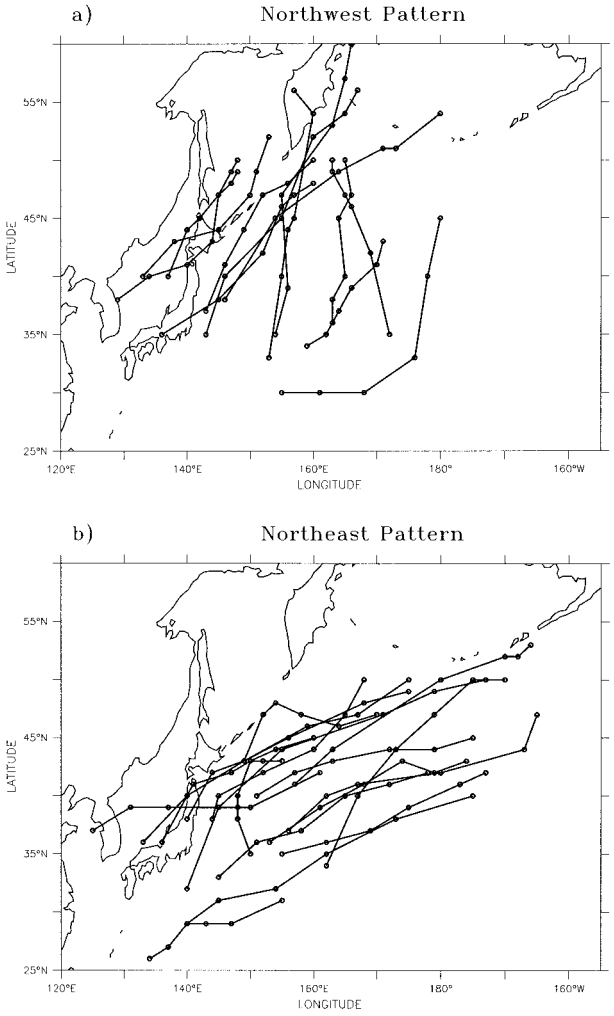

FIG. 2. Tracks of tropical cyclones that underwent extratropical transition between Jun–Oct 1994–98 in (a) a northwest pattern and (b) a northeast pattern. Points mark the positions every 12 h from 12 h before to 48 h after the time of transition.

by radius) in the cylindrical storm-following coordinate system and the divergence of the EP flux vector. Such a framework is analogous to the original designation of the divergence of the EP flux as a forcing of changes in the general circulation mean flow due to eddy activity (Eliassen and Palm 1961). The EP flux vector in the isentropic coordinate system is defined in the cylindrical grid as

$$\mathbf{P} = \left[-r\overline{(\sigma u)'v'},\ p'\overline{\frac{\partial M'}{\partial \lambda}} \right], \tag{1}$$

such that r is radius, p is pressure, λ is the azimuthal coordinate, an overbar represents an azimuthal average, and a primed value is the deviation from the azimuthal average. Since the first (radial) component of this vector is the eddy angular momentum flux and the second (vertical) term is the eddy heat flux, an EP flux vector that is nearly horizontal (vertical) reflects a dominant contribution from the eddy angular momentum (heat) fluxes. Scaling of the EP flux vector follows Edmon et al. (1980) in that the radial component is scaled by the actual length on the appropriate figure that represents 1 m and the vertical component is scaled by the length on the diagram that represents 1 K. The EP flux divergence was computed as

$$\nabla \cdot \mathbf{P} = \frac{1}{r}\left[\frac{\partial(r^2\overline{(\sigma u)'v'})}{\partial r}\right] + \frac{\partial\overline{(p'\partial M'/\partial\lambda)}}{\partial\theta}. \tag{2}$$

The divergence of the EP flux is related to the radial transport of PV (Edmon et al. 1980). Molinari et al. (1995) define this relationship as

$$-\frac{r\overline{\sigma^2}}{g}\langle u^*\Pi^*\rangle = \nabla \cdot \mathbf{P} - \frac{\partial\overline{(r\sigma'v')}}{\partial t}, \tag{3}$$

such that the angle brackets represent a pseudodensity-weighted azimuthal mean and the asterisk represents a deviation from that mean. Molinari et al. (1995) stress that the relationship between the mean tangential wind and the EP flux divergence or radial PV flux provides a physically based analysis of the relationship between the environment PV distribution and the total TC circulation. Specifically, the changes in the mean tangential wind at lower and upper levels are related to the radial PV fluxes, which are compared with the divergence of the EP flux.

a. Northwest circulation pattern: TY David

The PV distribution at 345 K (Fig. 3) was chosen to depict the relationship between the decaying TC with the upper-level midlatitude circulation pattern. During 0000–1200 UTC 19 September (Figs. 3a,b), David was east of the primary midlatitude PV reservoir associated with the trough that was approaching from the west. At 0000 UTC 20 September, the low-level (i.e., 315 K) PV signature of David (not shown) increased from 1.5 to 2 PVU and both the low-level (not shown) and upper-level (Fig. 3c) became connected to the region of high PV associated with the midlatitude circulation to the northwest. During the ensuing 12 h (Fig. 3d), the coupling between the midlatitude circulation and the now reintensifying extratropical cyclone to the south of the Kamchatka peninsula became more evident.

This connection between TY David and the midlatitude circulation is displayed in the vertical cross sections (Fig. 4) oriented from the southeast through David to the region of maximum midlatitude PV northwest of David. At 1200 UTC 19 September (Fig. 4a), David was still separate from the primary midlatitude circulation and baroclinic zone. During the following 12 h (Fig. 4b), the PV signature of David became connected to the midlatitude circulation at upper levels. Notice that the circulation above 335 K appears to slope northwestward toward the upper-level midlatitude trough.

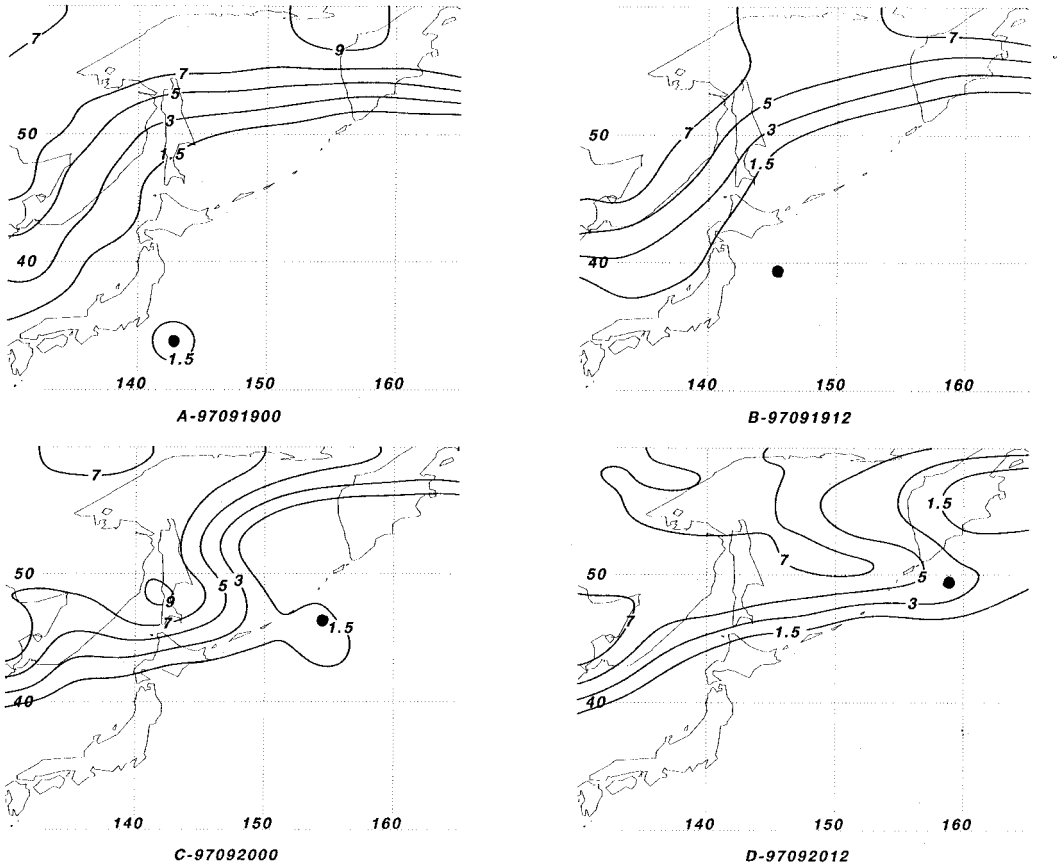

FIG. 3. Ertel potential vorticity on the 345 K isentropic surface for TY David at times (year, month, day, hour) indicated under each panel. Contours at 1.5 PVU (10^{-6} m^2 K s^{-1} kg^{-1}) and 3 PVU then in 2-PVU increments. The black circle in each panel marks the low-level center of David.

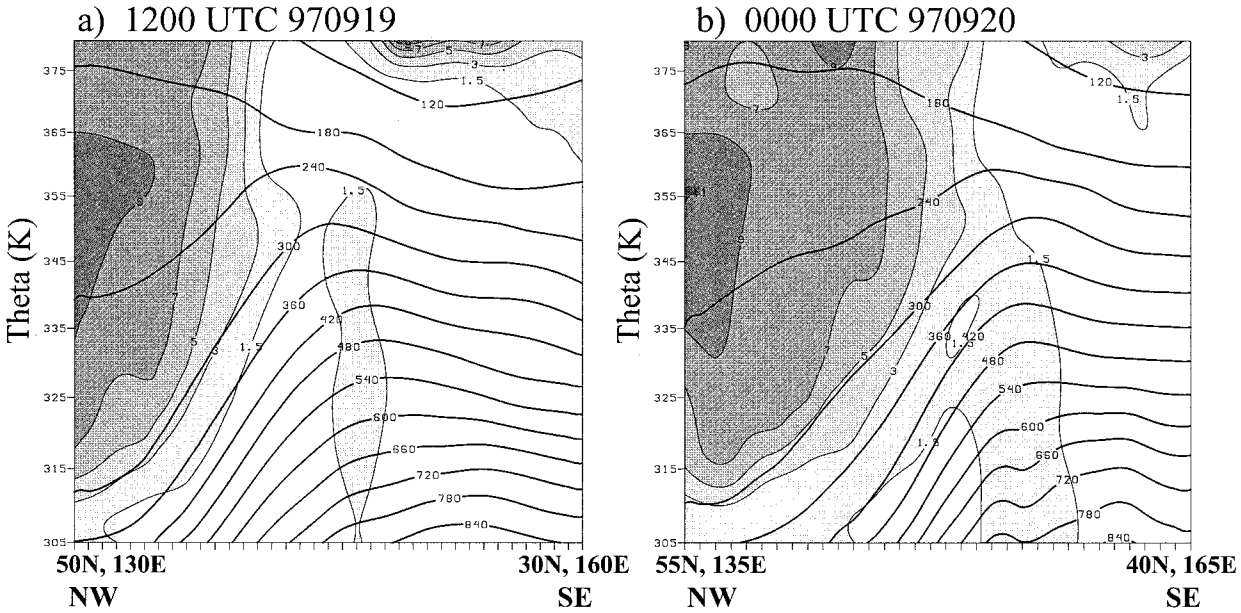

FIG. 4. Vertical cross sections of potential vorticity (thin lines and shaded) and pressure surfaces (dark lines) for (a) 1200 UTC 19 Sep and (b) 0000 UTC 20 Sep 1997. Potential vorticity contours as in Fig. 3 and pressure contours are in 60-hPa increments. The cross sections are oriented from northwest to southeast through the David circulation.

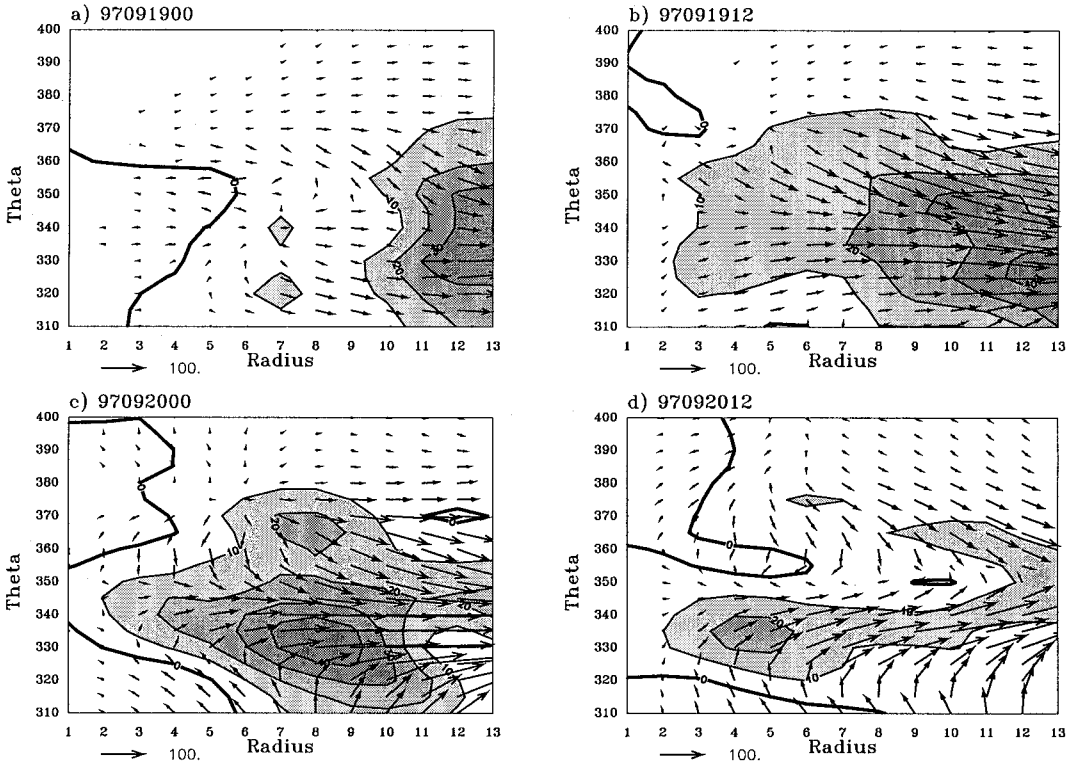

FIG. 5. Cross section (in radius and potential temperature) of Eliassen–Palm flux vectors and the divergence of the vectors at the times (year, month, day, hour) indicated above each panel. The divergence contour interval is 10^4 hPa m^2 K^{-1} s^{-2}. The vertical component (hPa m^3 K^{-1} s^{-2}) is multiplied by the length on the diagram that is equal to 1 K, and the horizontal component (hPa m^3 s^{-2}) is multiplied by the length on the diagram equal to 1 m.

The dynamic tropopause may be defined physically as a boundary between the larger PV values of the stratosphere from the smaller PV values in the troposphere and is defined here by the 1.5-PVU contour (Bosart and Lackmann 1995) in the environment away from the David circulation. Hirschberg and Fritsch (1991a,b) have associated a steep tropopause slope with upstream trough development and cyclogenesis. At the time of the ET of David (Fig. 4b), the tropopause sloped from above 375 K (approximately 100 hPa) southeast (i.e., downstream) of David to below 315 K (approximately 600 hPa) northwest (i.e., upstream) of David.

As indicated above, the EP fluxes describe the influence of the environmental PV distribution on the TC via eddy heat and angular momentum fluxes. At 0000 UTC 19 September (Fig. 5a), the maximum EP flux divergence was more than 10° lat radius from the center of David. The primarily horizontal vectors at this time implied that the dominant influence of the eddy momentum fluxes was due to the mutual approach of the decaying TC and midlatitude trough. At 1200 UTC 19 September (Fig. 5b), the EP flux divergence was closer to the center of David and the horizontal orientation and magnitude of the vectors increased as the midlatitude trough and TC approached. These patterns of EP vectors and associated flux divergence are similar to those computed by Molinari et al. (1995) when Hurricane Elena began to interact with an upper-level trough. At 0000 UTC 20 September (Fig. 5c), the EP flux divergence was concentrated near 335 K between 6° and 10° lat from the center of David. However, large vertical components below 330 K indicated that positive eddy heat fluxes began to increase at the lower levels, which implies that baroclinic energy conversions started to influence the decaying TC. Above 330 K, eddy angular momentum fluxes were still large as the interaction with the upper-level trough continued.

This pattern of EP vectors during the reintensification stage of ET is very different from those associated with Hurricane Elena, for which eddy angular momentum fluxes associated with the upper-level trough (Molinari et al. 1995) contributed to an increase in upper-level cyclonic tangential winds. During the transition of TY David, eddy heat fluxes began to dominate in the mid- and low levels. Examination of the spatial distribution of the vertical component of the EP flux vector at 315 K (Fig. 6a), and the pressure deviations from the azimuthal average (Fig. 6b) at 315 K, helps to explain the vertical EP flux components. The coldest air (i.e., largest negative pressure deviation) was located northwest of David (Fig. 6b), which coincided with the location of the midlatitude trough, and the warmest air was located

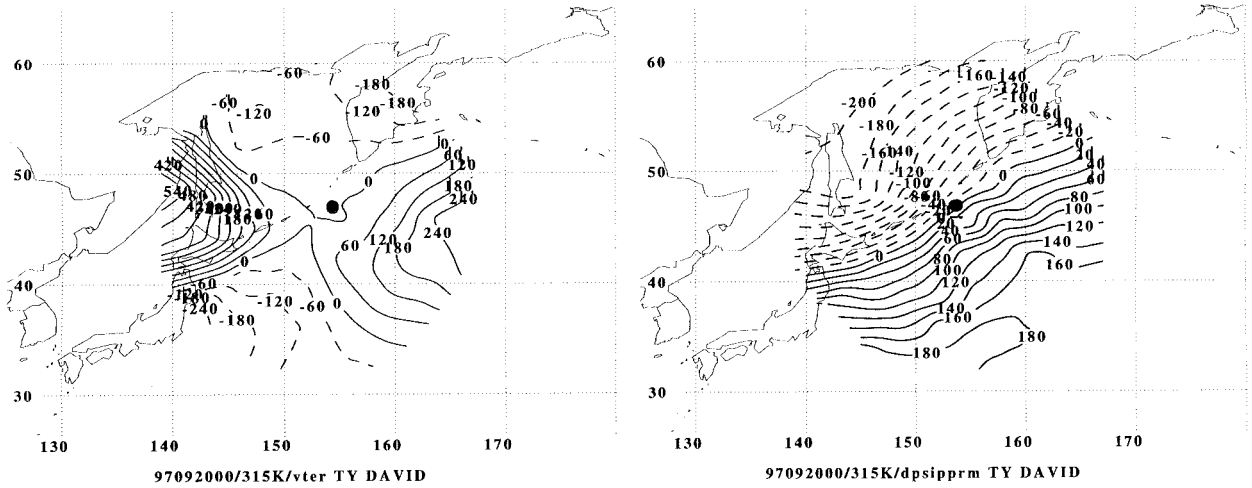

FIG. 6. (a) The vertical component (hPa m^3 K^{-1} s^{-2}) of the Eliassen–Palm vectors at 315 K on the cylindrical grid that is centered on the David circulation at 0000 UTC 20 Sep 1997. (b) The pressure deviation (hPa) from the azimuthal average over the cylindrical grid at 315 K. The black dot marks the center of David.

to the southeast of David. Therefore, the eddy heat fluxes (Fig. 6a) were due to cold (warm) advection to the northwest (northeast) of the center of the weakening TC.

The environmental interactions defined by the pattern of EP flux divergence, which are related to the eddy flux of PV, influence the evolution of tangential wind during the ET process. Although a strong low-level baroclinic component is part of the environmental influence on David at the time of ET (Fig. 5c), the EP flux divergence remained concentrated between 330 to 350 K and 4° to 11° lat from the center. At these levels, this corresponded to a change in the tangential wind distribution (Fig. 7a) from maximum cyclonic winds within 3° lat radius of the circulation center (based on relatively coarse NOGAPS analysis) and anticyclonic winds at outer radii to a more broad cyclonic wind distribution. As a closed upper-level midlatitude cyclonic circulation became superposed over the David circulation, the radial PV flux increased between 5° and 9° lat radius (Fig. 7b).

By 1200 UTC 20 September (Fig. 5d), the maximum in EP flux divergence moved closer to the circulation center but decreased in magnitude. The eddy heat flux contributions below 330 K increased and also moved closer to the circulation center as thermal advection continued to increase. However, the decrease in overall EP flux divergence was due to the decrease in the eddy angular momentum component (horizontal component), which was consistent with the near-vertical alignment of the lower- and upper-level circulations.

b. Northeast circulation pattern: TY Opal

Interaction between TY Opal and the midlatitude circulation began when Opal crossed eastern Japan between 0000 and 1200 UTC 20 June (Figs. 8a,b) ahead of an eastward-moving midlatitude trough. During these 12 hours, the tongue of upper-level PV associated with the midlatitude trough approached the decaying TC. Unlike the case of TY David, the primary midlatitude PV reservoir was northeast of Opal rather than being to the northwest associated with the approaching midlatitude trough. At 0000 UTC 21 June, the upper-level PV distribution (Fig. 8c) near Opal continued to stretch zonally toward Opal with the increase in the strong zonal flow across the Sea of Japan that broadened the midlatitude trough structure. By 1200 UTC 21 June (Fig. 8d), the separation between the region of upper-level PV and Opal increased as Opal moved more rapidly eastward and northward toward the primary midlatitude circulation to the northeast.

Opal approached a midlatitude circulation pattern that was very different from the pattern associated with the transition of David. A vertical cross section from the southwest to northeast through Opal at 1200 UTC 20 June (Fig. 9a) indicated that the baroclinic zone associated with the preexisting midlatitude cyclone was about 15° lat northeast of the Opal circulation. At 0000 UTC 21 June (Fig. 9b), Opal was still well separated from the primary midlatitude circulation and baroclinic zone.

As Opal moved northward, a maximum in the pattern of EP flux divergence first appeared at outer radii above 330 K (not shown) and the leading edge of the maximum moved inward to within 3° lat of the center at 0000 UTC 20 June (Fig. 10a) as TY Opal and the upper-level trough began to interact. The maximum in EP flux divergence continued to propagate inward at 1200 UTC 20 June (Fig. 10b), which corresponded to a short-lived increase in upper-level tangential winds (not shown). Since the eddy heat flux contributions remained small at low levels, baroclinic energy processes were not as significant as were the strong angular momentum fluxes associated

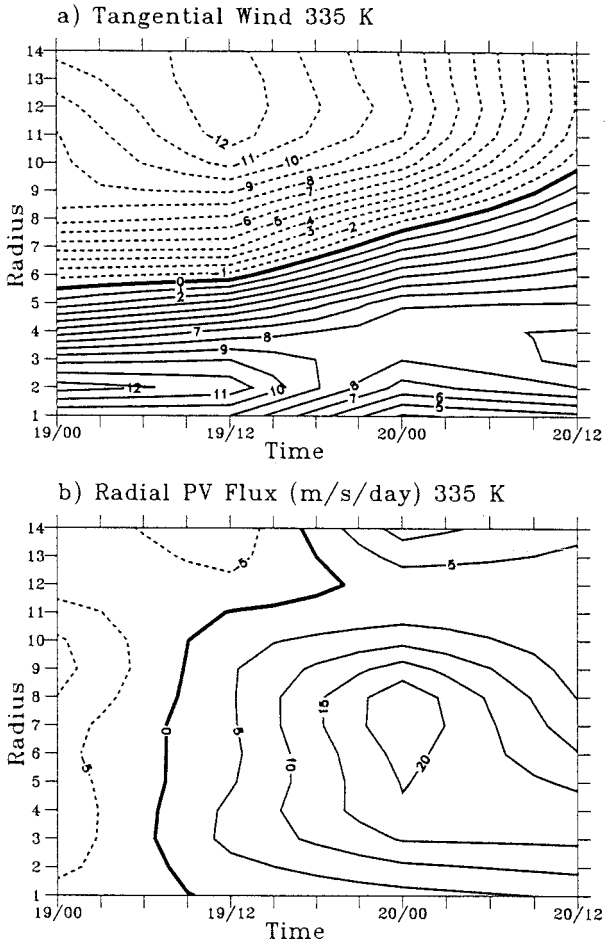

FIG. 7. Time (12-h increments) and radius (° lat) distribution of (a) tangential wind (m s^{-1}) and (b) radial potential vorticity flux (m s^{-1} d^{-1}) at 335 K.

with the zonal flow off the Asian mainland. At 0000 UTC 2100 (Fig. 10c), the EP flux divergence decreased at radii smaller than 6° lat evidently because of the decrease in the intensity of the upper-level trough as well as the increased separation distance between Opal and the trough. That is, the maximum EP flux divergence descended at outer radii as the remnants of Opal began to move toward the midlatitude cyclone to the northeast. A slight increase in the vertical component to the EP vectors became evident below 330 K and beyond 9° lat radius. This contribution to the vertical component of the EP flux vector was associated with the advection of cold and warm air related to the midlatitude cyclone to the northeast (see Fig. 11), rather than with the thermal advection caused by the decaying TC encroaching on the midlatitude baroclinic zone, as was found to be associated with the transition of David. By 1200 UTC 21 June (Fig. 10d), Opal came under the influence of the midlatitude cyclone to the northeast, and the EP vectors became disorganized at low levels and the flux divergence decreased.

5. Kinetic energy budget

The evolutions of kinetic energy and forcing mechanisms responsible for changes in kinetic energy during the northwest and northeast ETs of David and Opal were examined via an Eulerian kinetic energy budget equation:

$$\frac{\partial K}{\partial t} = \underbrace{\int -\mathbf{V}\cdot\nabla\phi}_{\text{GKE}} + \underbrace{\int -\nabla\cdot k\mathbf{V}}_{\text{HFC}} + \underbrace{\int -\frac{\partial \omega k}{\partial p}}_{\text{VFC}} + \underbrace{\int k_0\frac{\partial p_0}{\partial t}}_{\text{Bd}} + \underbrace{\int \mathbf{V}\cdot\mathbf{F}}_{D}. \quad (4)$$

In Eq. (4), and in the definition of K below, a shorthand notation is used in which a single integral sign is used to denote

$$\frac{1}{gA}\int_p\int_A dA\, dp.$$

also:

V is the horizontal wind vector,
A is the horizontal area of integration,
ω is the vertical motion in isobaric coordinates,
k is the horizontal kinetic energy per unit mass,
K is the total energy content equal to $\int k$,
$\phi = gz$ such that z is the geopotential height,
F represents the frictional forces, and
k_0, p_0 are values of k and pressure at the lowest level.

All operations are performed on pressure surfaces. This budget relates the time rate of change of kinetic energy per unit area (left side) over an open region due to a collection of sources and sinks. The first term on the right side, labeled GKE, is the net generation (destruction) of kinetic energy associated with cross-isobaric flow to lower (higher) pressure. The second term, labeled HFC, is the horizontal flux convergence of kinetic energy from the surrounding region into the volume, and the third term, labeled VFC, is the vertical flux convergence. Whereas the fourth term, labeled Bd, is related to changes in the mass of the volume, this term will be ignored since the kinetic energy values at the lowest level are small and the upper level is fixed at 100 hPa. The final term on the right-hand side, labeled D, represents the dissipation of kinetic energy, which in this study must be calculated as a budget residual from the remaining terms that are computed from the NOGAPS analyses. The kinetic energy budget is computed on a 25° lat–long grid with the center of the decaying TC always in the middle of the grid.

a. Northwest circulation pattern: TY David

The kinetic energy budget is evaluated for TY David from 0000 UTC 19 September through 1200 UTC 20

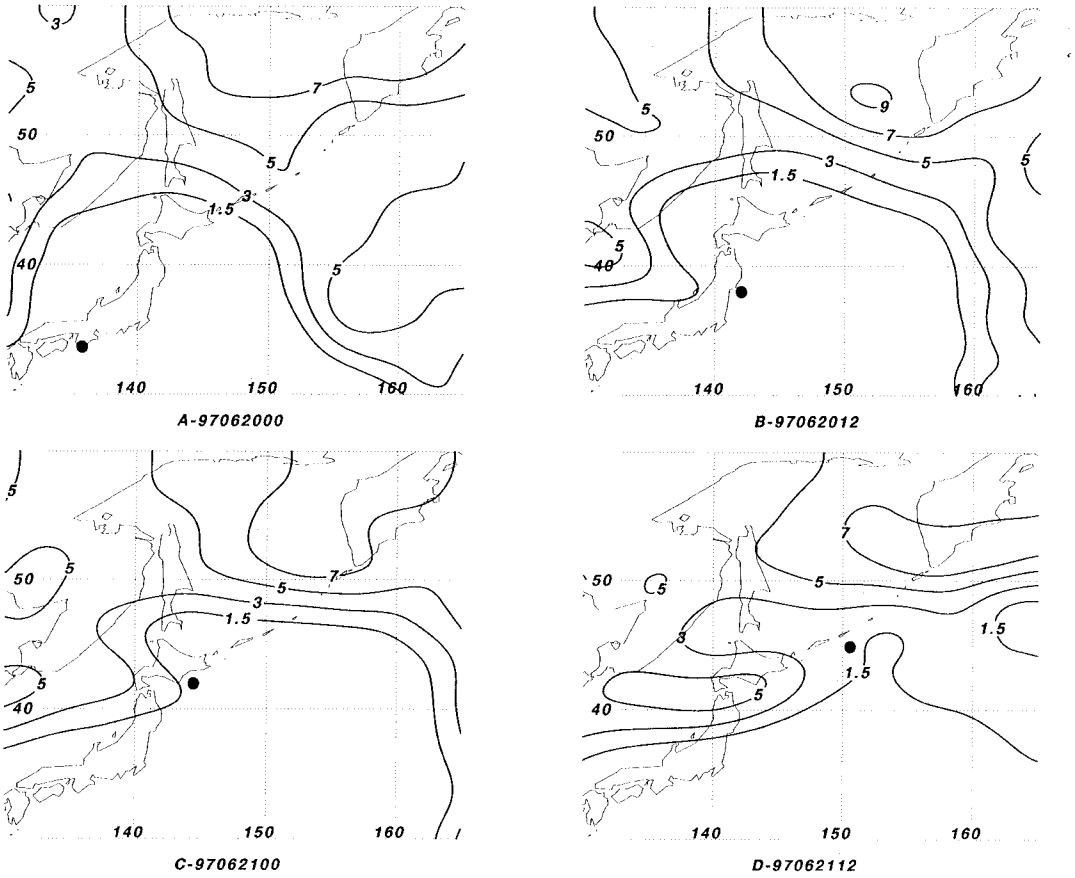

FIG. 8. Ertel potential vorticity on the 345 K isentropic surface as in Fig. 3, except for the times associated with the transition of TY Opal as indicated beneath each panel. The black circle in each panel marks the low-level center of Opal.

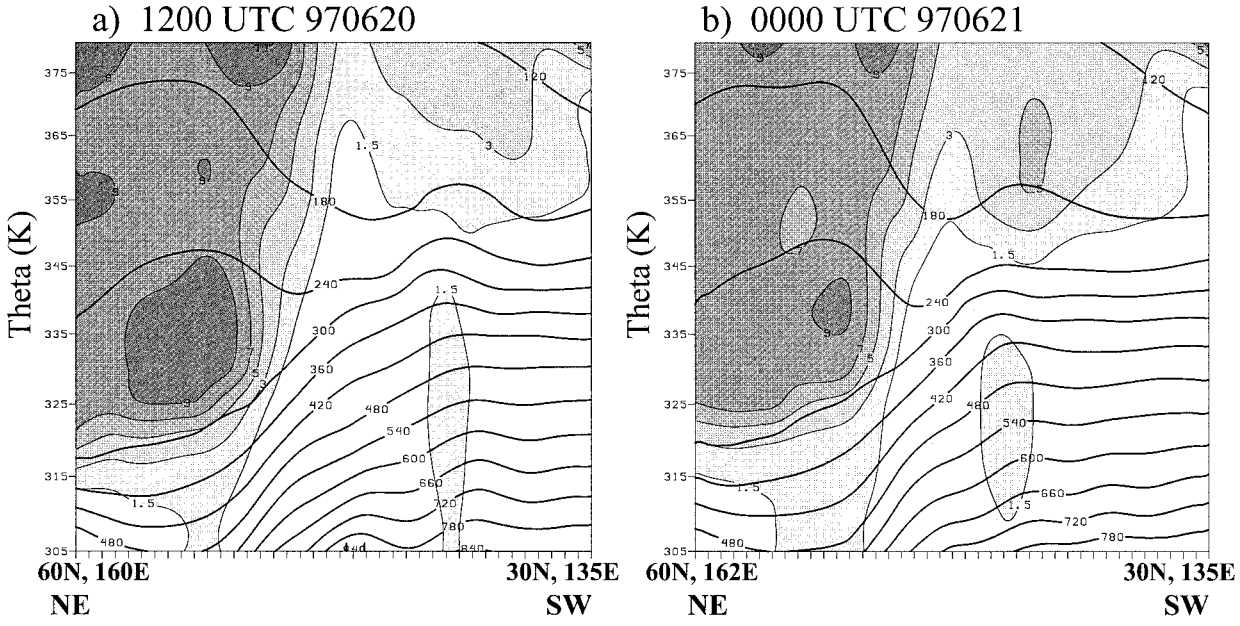

FIG. 9. Vertical cross sections of potential vorticity and pressure as in Fig. 4, except for TY Opal at the times indicated above each panel.

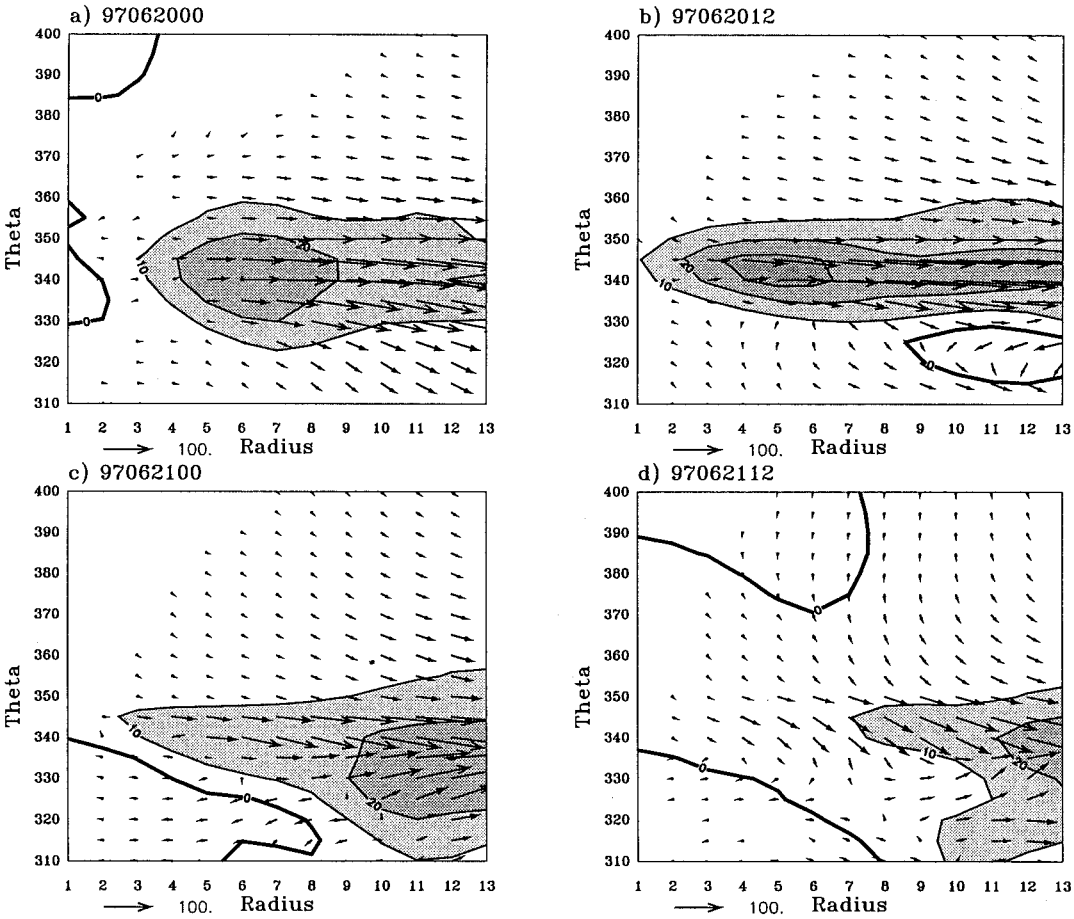

FIG. 10. Cross section of Eliassen–Palm flux vectors and the divergence of the vectors as in Fig. 5, except for the times (year, month, day, hour) associated with the transition of TY Opal as indicated above each panel.

September and the area-mean values are calculated on pressure surfaces from 1000 to 100 hPa and vertically integrated (Table 1). Even though the inner-core winds of David were decaying, an increase in total kinetic energy in the volume occurred during the reintensification of David as an extratropical cyclone. The maximum kinetic energy occurred at 0000 UTC 20 September and began to decrease afterward when the extratropical cyclone became vertically stacked (Harr and Elsberry 2000). The time rate of change of kinetic energy was a maximum at 1200 UTC 19 September, which is defined by Klein et al. (2000) as the start of the reintensification period and is also when the frontogenesis parameter defined by Harr and Elsberry (2000) began to increase dramatically. Through the initial 36 h, the HFC was a kinetic energy sink while the GKE term was a source of kinetic energy. Both the HFC sink of kinetic energy and the GKE reached a maximum at 1200 UTC 19 September. The physical mechanisms associated with these terms will be discussed in detail below. The inferred dissipation of kinetic energy was maximum at 0000 UTC 20 September, which was immediately following the period of largest deepening of the extratropical cyclone.

Harr and Elsberry (2000) found that the greatest frontal structural changes during the ET of David occurred during the period of 1200 UTC 19 September to 0000 UTC 20 September. The vertical distribution of each term in the kinetic energy budget (Fig. 12) indicates that the largest values of all terms except dissipation occurred in the upper troposphere near 250 hPa. While the time rate of change of kinetic energy was positive at all levels (1000–100 hPa) at 1200 UTC 19 September (Fig. 12a), it became negative at upper levels during the

TABLE 1. Kinetic energy budget as in Eq. (4) for TY David integrated from 1000 to 100 hPa. Kinetic energy (K) is in 10^5 J m^{-2}, and changes in K are in W m^{-2}.

Date	K	$\partial K/\partial t$	HFC	GKE	$D(k)$
0000 UTC 19 Sep 97	6.9	2.9	−14.0	27.5	10.6
1200 UTC 19 Sep 97	10.1	6.8	−20.1	43.3	16.4
0000 UTC 20 Sep 97	13.1	2.6	−13.9	41.9	25.4
1200 UTC 20 Sep 97	12.0	−0.15	1.2	16.1	17.4

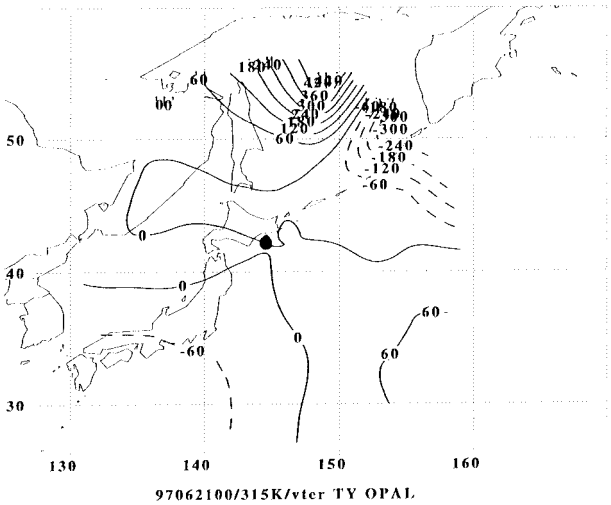

FIG. 11. Vertical component of the Eliassen–Palm vectors as in Fig. 6a, except for TY Opal at 315 K at 0000 UTC 21 Jun 1997. The black dot marks the center of Opal.

next 12 h (Fig. 12d). Eventually, the time rate of change of kinetic energy became negative at all levels as reintensification slowed by 1200 UTC 20 September (Table 1). Between 1200 UTC 19 September and 0000 UTC 20 September, the removal of kinetic energy at upper levels due to HFC (Figs. 12b,e) was offset primarily by GKE (Figs. 12c,f) with smaller contributions from the upward transport of energy from below (negative VFC) and downward transport from above (positive VFC; Figs. 12b,e). The transport from below was upward due to the vertical motion and convection associated with the decaying TC. The sink of kinetic energy due to the HFC may be attributed to the strong upper-level winds that exited the region northeast of David (Fig. 13). The outflow from David appeared to contribute to increased southwesterly winds in the midlatitude trough, which also placed David near the right entrance region of an upper-level jet streak. Whereas Chien and Smith (1977) and DiMego and Bosart (1982b) found HFC to be a source of energy due to a strong jet streak entering the domain of the decaying TC, the jet associated with this case of ET over the western North Pacific contributed to a kinetic energy decrease in the volume. Based on the analysis of Klein et al. (1999) cases of ET over the western North Pacific that resulted in reintensification as an extratropical cyclone exhibited enhanced upper-level winds immediately east (downstream) of the decaying TC.

The energy source due to the GKE term had a maximum in both the lower troposphere and at upper levels (Figs. 12c,f). At upper levels, the generation of kinetic energy associated with winds crossing from higher to lower heights (Fig. 13) was partially offset by the horizontal export of energy from the domain. At lower levels, the generation of kinetic energy was primarily offset by the residual dissipation term, which indicated the dominance of surface drag.

To examine the sources and sinks of kinetic energy more fully, the budget terms were partitioned (Chen et al. 1978; DiMego and Bosart 1982b) into contributions from the divergent wind ($\mathbf{V}_d$) and contributions from the nondivergent wind ($\mathbf{V}_r$). For this partition, the total wind was defined as

$$\mathbf{V} = \mathbf{V}_d + \mathbf{V}_r. \tag{5}$$

The divergent wind component was obtained from

$$\mathbf{V}_d = \nabla\chi, \tag{6}$$

with the velocity potential χ defined from

$$\nabla^2\chi = \frac{\partial u}{\partial x} + \frac{\partial v}{\partial y}. \tag{7}$$

The nondivergent wind was defined as

$$\mathbf{V}_r = \mathbf{k} \times \nabla\psi, \tag{8}$$

with the streamfunction ψ defined from

$$\nabla^2\psi = \frac{\partial v}{\partial x} - \frac{\partial u}{\partial y}. \tag{9}$$

Nearly all of the kinetic energy sink due to the HFC export of energy from the region was by the nondivergent wind (Table 2). During the final 12 h of the period (1200 UTC 20 September), the HFC of kinetic energy became small when the upper- and lower-level circulations started to become aligned in the vertical. At both 0000 UTC 19 September and 0000 UTC 20 September, approximately one-third of the generation of kinetic energy was due to the divergent wind. The generation of kinetic energy at low levels (Fig. 14) may be attributed to dynamically and frictionally induced cross-isobaric flow as the divergent wind blew from higher to lower heights (not shown). At upper levels, the larger generation of kinetic energy associated with the nondivergent wind directed from higher to lower heights downstream of the reintensifying circulation also contributed to the acceleration of upper-level winds over that region (Fig. 13). A relative maximum contribution to GKE at upper levels by the divergent wind was due to upward motion associated with David that contributed to a velocity potential maximum and divergent winds toward lower heights (not shown).

In summary, a net export of kinetic energy from the volume at upper levels was balanced by a generation of energy due to cross-contour flow (primarily by the nondivergent wind) and vertical transport of energy to the upper levels. The dominance of the kinetic energy sources at upper levels was reflected by an accumulation of energy as the circulation intensified. Coupling of David with the northwest circulation pattern contributed to energy sources and sinks when the outflow from David also contributed an upper-level wind maximum over the downstream portion of the midlatitude trough, such that

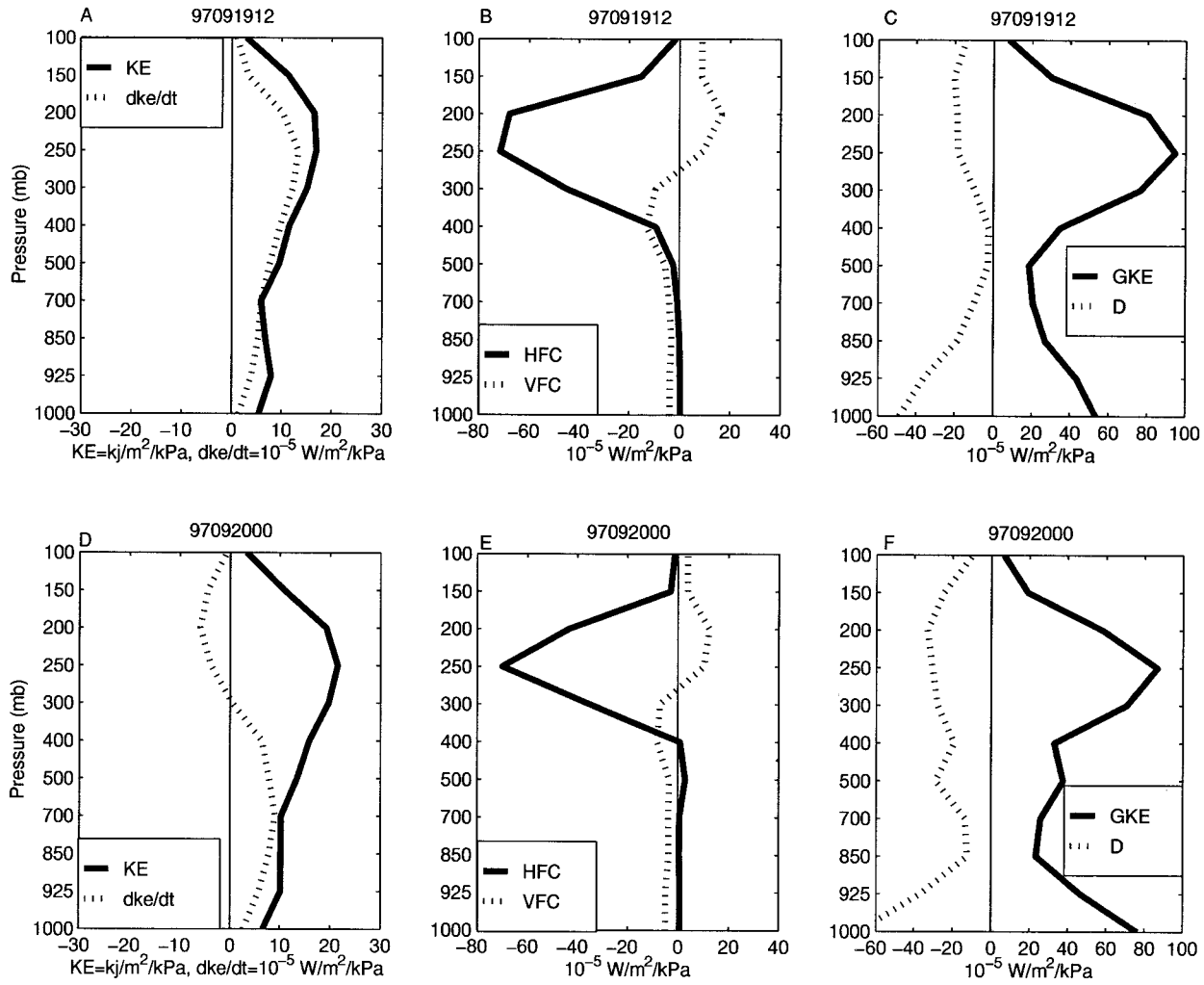

FIG. 12. Vertical distributions of the terms in the kinetic energy budget equation [(4) in text] for TY David at the times indicated above each panel. Kinetic energy is in units of kJ m^{-2} kPa^{-1} and changes in kinetic energy are in 10^{-5} W m^{-2} kPa^{-1}.

the reintensifying circulation was below the right-rear quadrant of the wind maximum.

Harr and Elsberry (2000) showed how the coupling of the TC and the midlatitude trough via vertical circulations contributed to frontogenesis and led to structural characteristics typically associated with an extratropical cyclone. Similarly, these vertical circulations generated during interactions between the TC and midlatitude trough during the northwest ET impact the energetics pattern. After transforming the GKE term as

$$\mathbf{V} \cdot \nabla\phi = \nabla \cdot (\phi\mathbf{V}) - \phi\nabla \cdot \mathbf{V}, \tag{10}$$

and noting that

$$\phi\nabla \cdot \mathbf{V} = -\frac{\partial(\omega\phi)}{\partial p} - \omega\alpha, \tag{11}$$

and $\omega\alpha = RT/p$, an explicit contribution to GKE by the vertical circulation may be defined (Palmen 1958; Newton 1990). During 1200 UTC 19 September and 0000 UTC 20 September (Fig. 15), the vertical circulations contributed to generation (destruction) of kinetic energy northeast (southwest) of David. As defined by the pattern of ageostrophic winds in Fig. 15, sinking motion in the thermal trough (Harr and Elsberry 2000) coincided with a deceleration of the winds that entered the region from the west and rising motion in the thermal ridge coincided with the acceleration of winds that exited the region to the east. Therefore, the kinematics associated with the coupling of the TC and midlatitude trough also contributed to kinetic energy generation and reintensification of the circulation as an extratropical cyclone. The kinetic energy was derived from solenoidal circulations that were a manifestation of the coupling between the TC and trough, with cold air sinking to the west and warm air rising to the east that act to convert available potential energy into kinetic energy.

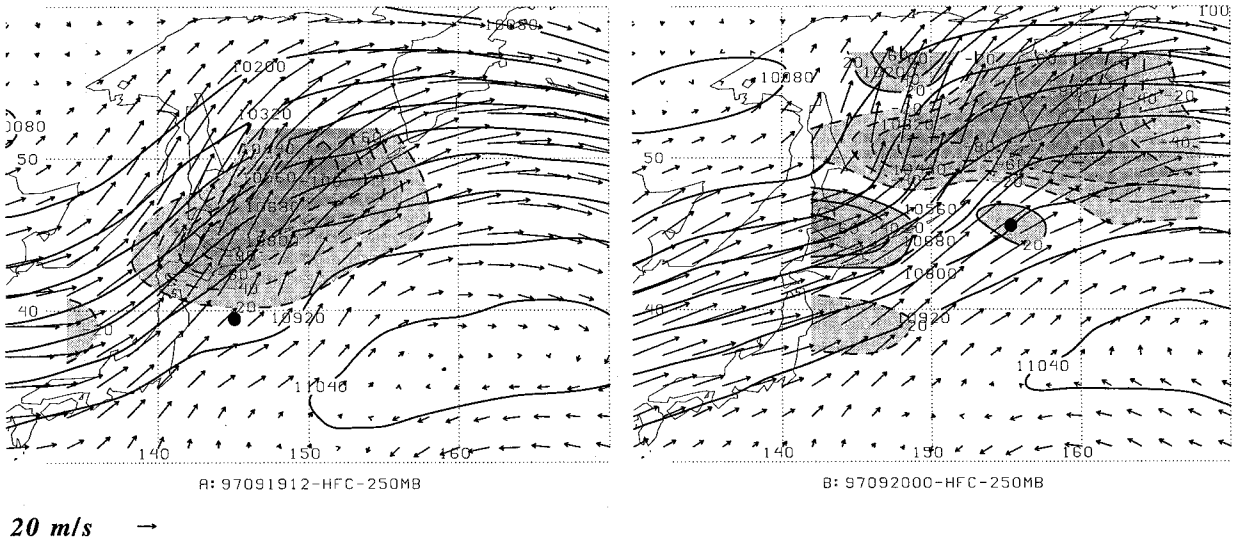

FIG. 13. Analyzed heights (m, solid contours) at 250 mb, winds (m s^{-1}, arrows, scale at bottom left), and horizontal flux convergence of kinetic energy (10^{-5} W m^{-2} kPa^{-1} shaded contours, negative contours are dashed) for (a) 1200 UTC 19 Sep and (b) 0000 UTC 20 Sep. The black circle in each panel marks the low-level center of David.

b. Northeast circulation pattern: TY Opal

Vertically integrated values of kinetic energy and changes in kinetic energy (Table 3) associated with the ET of Opal exhibited characteristics similar to those associated with David except the magnitudes were smaller, which was likely due to the less baroclinic conditions during June. The time rate of change of kinetic energy was maximum at the time that Klein et al. (2000) define reintensification to begin and the frontogenesis parameter in Harr and Elsberry (2000) began to increase dramatically. The energy sink due to the horizontal export of energy out of the region tended to offset some of the generation of energy. The frictional dissipation magnitudes, which were estimated as residuals, were generally proportional to the generation until the total kinetic energy reached a maximum.

During the period 1200 UTC 20 June and 0000 UTC 21 June (Figs. 16a,d), the magnitude of kinetic energy was again largest in the upper troposphere. Outflow from Opal again contributed to a transport of kinetic energy away from the region (Figs. 16b,e). The generation of kinetic energy (Figs. 17c,f) profile had maxima at low and upper levels. As in the David case (Fig. 14), the generation of energy at upper levels due to cross-contour flow to lower heights as part of the outflow also contributed to the export of energy away from Opal. The primary contribution to the energy sink due to horizontal export from the region around Opal was due to the nondivergent winds (Table 4), which was similar to that found with David. Such a contribution might be expected to occur in all ET cases due to the upper-level structure of the TC outflow.

Major differences between David and Opal were found in the generation of kinetic energy due to the divergent wind and nondivergent winds (Table 4), and these differences may be related to the northwest or northeast circulation patterns into which the TCs are moving. Whereas the primary generation of kinetic energy during the ET of Opal was from the divergent wind, the nondivergent wind contribution was negative at two of the four times. In David (Table 2), the nondivergent GKE term was larger than the divergent GKE term and contributed nearly two-thirds of the energy source. From the vertical distribution of the partition of GKE (Fig. 17), the largest generation of kinetic energy was by the divergent wind at low levels due to dynamic and frictional convergence. As in the David case (Fig. 14), the divergent wind aloft also contributed to a secondary maximum in kinetic energy generation. However, the nondivergent contribution to kinetic energy generation at upper levels in Opal was negative (e.g., energy sink), while it constituted the primary energy source during the ET of David. Examination of the distribution of the kinetic energy production via the nondivergent wind at 400 hPa (Fig. 18) indicated that the negative kinetic energy generation in the volume was due to the decel-

TABLE 2. The horizontal flux convergence of kinetic energy due to the total wind (HFC), the nondivergent (HFC_r, and the divergent wind (HFC_d). The generation of kinetic energy due to the total wind (GKE), the nondivergent wind (GKE_r), and the divergent wind (GKE_d). All quantities are for TY David at the times shown, and are integrated from 1000 to 100 hPa with units of W m^{-2}.

Date	HFC	HFC_r	HFC_d	GKE	GKE_r	GKE_d
0000 UTC 19 Sep 97	−14.0	6.8	7.2	27.5	19.0	8.5
1200 UTC 19 Sep 97	−20.1	−12.4	−7.6	43.3	29.1	14.2
0000 UTC 20 Sep 97	−13.9	−14.1	0.2	41.9	26.5	15.4
1200 UTC 20 Sep 97	1.2	−2.9	4.1	16.1	14.7	1.4

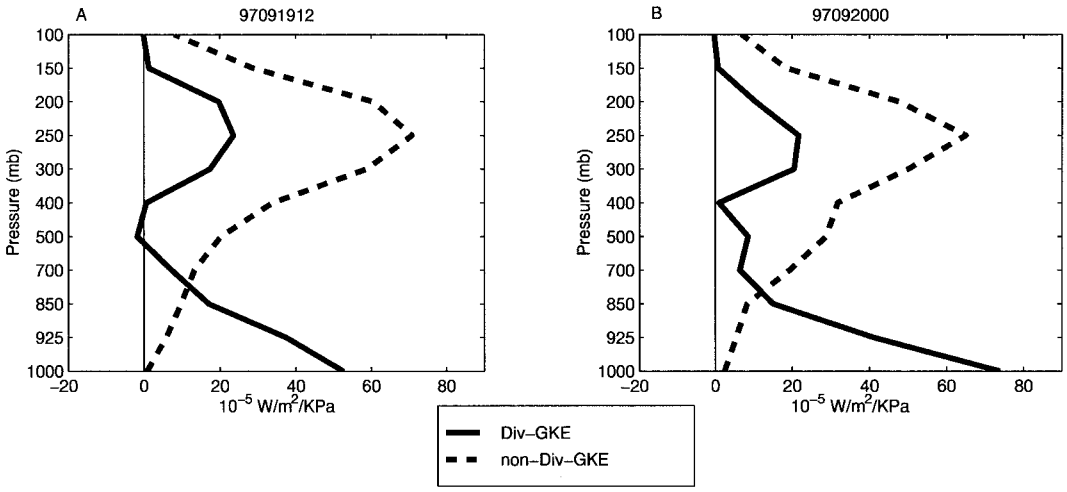

FIG. 14. Vertical distribution of the generation of kinetic energy (10^{-5} W m^{-2} kPa^{-1}) due to the divergent (solid lines) and nondivergent (dashed lines) winds for TY David at the times indicated above each panel.

eration and turning toward higher heights of the northerly and northwesterly winds associated with the large midlatitude cyclone northeast of Opal. Therefore, the movement of Opal toward the midlatitude cyclone led to a destruction of kinetic energy at the interface between the two circulations and prevented a contribution to kinetic energy production at upper levels, which was the primary energy source during the ET of David into the northwest pattern.

Recall that at 1200 UTC 20 June Opal was beginning to couple with the midlatitude trough over Japan. Examination of the conversion from potential energy to kinetic energy via vertical circulations (Fig. 19) indicated that sinking motion in the thermal trough west of Opal (see Harr and Elsberry 2000) coincided with the deceleration of winds over Japan. Rising motion in the thermal ridge east of Opal coincided with an acceleration of winds to the northeast of Opal. Twelve hours later (Fig. 19b), the primary linkage via vertical circulations occurred between Opal and the midlatitude cyclone to the northeast. Coupling with the thermal trough to the west of Opal was reduced greatly over the past 12 h (see Fig. 19a). Therefore, Opal interacted more with the preexisting midlatitude cyclone to the northeast than with the midlatitude trough to the west. This interaction lead to a region of kinetic energy reduction due to the deceleration of the winds around the midlatitude cyclone that approached Opal from the north and prevented kinetic energy generation with respect to Opal and the western midlatitude trough that had contributed to Opal's initial movement into the midlatitudes.

6. Discussion and conclusions

The purpose of this study has been to document how the reintensification stage of the ET of a TC is influenced by the primary midlatitude circulation pattern into which the decaying TC moves. Two characteristic midlatitude circulation patterns associated with ET cases of western North Pacific TCs are related to whether the primary midlatitude circulation is located to the northwest or the northeast of the TC. Extratropical transition associated with a northwest pattern occurs downstream of a midlatitude trough that is the primary midlatitude circulation over the western North Pacific region. The transforming circulation typically moves north–northeast during reintensification as an extratropical cyclone. Whereas a TC that undergoes ET into a northeast pattern also moves ahead of a midlatitude trough, the primary midlatitude circulation is a preexisting, quasi-stationary cyclone located northeast of the decaying TC. Typically, the decaying TC then moves eastward into the strong zonal flow between this preexisting midlatitude cyclone and the subtropical ridge to the southeast. After 36 h of reintensification as an extratropical cyclone, systems in a northwest pattern tend to have a statistically significant lower sea level pressure than those in a northeast pattern (Klein et al. 2000).

Two cases have been examined in detail with respect to the physical characteristics of each circulation pattern and its impact on ET over the western North Pacific. The transition of each cyclone into the two synoptic environments affects the heat and momentum fluxes between the cyclone and the environment, and the generation of kinetic energy during reintensification as an extratropical cyclone. As each TC moved poleward, eddy angular momentum fluxes, which were also related to eddy PV fluxes, were concentrated at upper levels similar to that calculated by Molinari et al. (1995) with respect to the intensification of Hurricane Elena due to a trough interaction. In the Elena case, an intense upper-level anticyclone that is a characteristic of a mature TC structure effectively reduced the dynamic scale of the upper-level trough such that a favorable interaction oc-

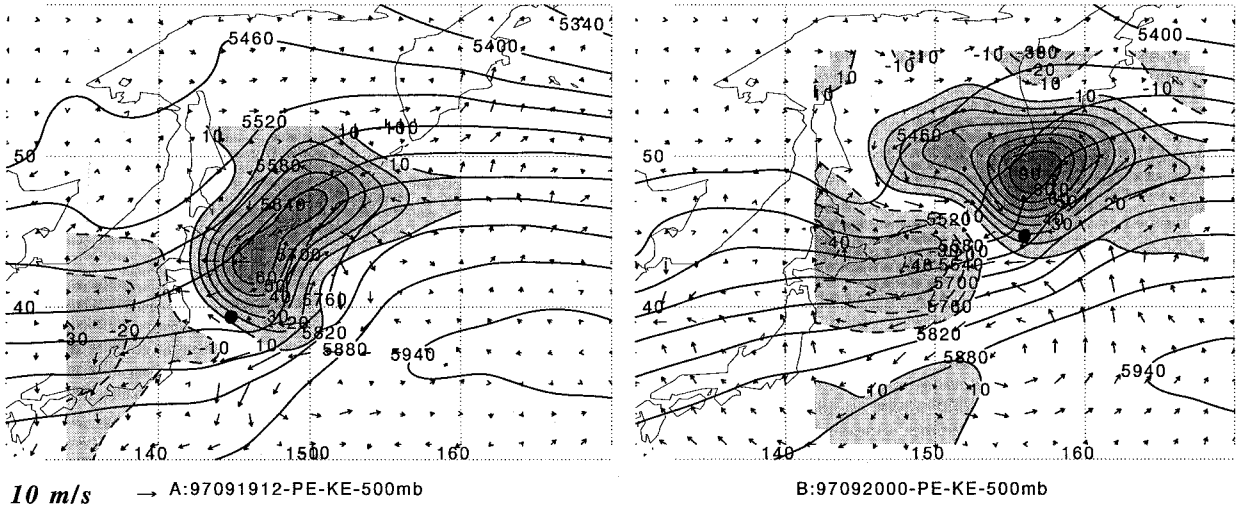

FIG. 15. Analyzed heights (m, solid contours) at 500 hPa, ageostrophic winds (m s^{-1} arrows, scale at bottom left), and conversion of available potential energy into kinetic energy (10^{-5} W m^{-2} kPa^{-1} shaded, negative contours are dashed) for (a) 1200 UTC 19 Sep and (b) 0000 UTC 20 Sep. The black circle in each panel marks the low-level center of David.

curred through transfer of eddy angular momentum (i.e., eddy PV flux). By contrast, the horizontal and vertical scales of the midlatitude troughs associated with these two cases of western Pacific ET were large compared with the equatorward extension of the trough that impacted Elena. Thus, the dynamic scale of both of these troughs remained larger than that of the TC, which then weakened and lost its tropical-like characteristics. The subsequent impact of the midlatitude trough with the weakening TC depends sensitively on the degree of coupling between the TC and midlatitude circulation. If the juxtaposition of the TC and midlatitude circulation leads to a dynamic linkage between the two, as in the David case (Fig. 9), development of the extratropical cyclone is expected.

Although the eddy angular momentum component of the EP flux was similar for both cases due to the movement of each TC toward a midlatitude trough, the character of the eddy heat flux contribution was very different for each case. The low-level thermal advection around David (northwest pattern) contributed to increased low-level eddy heat fluxes as ET began, which is a consequence of the direct coupling between the decaying TC and the baroclinic zone associated with the midlatitude circulation. These eddy heat fluxes are directly related to baroclinic energy conversions that contributed to the reintensification of the decaying TC into a significant extratropical cyclone with gale-force winds. During the poleward movement of Opal into a northeast circulation pattern, the eddy heat fluxes did not increase at low levels except at outer radii when the primary preexisting midlatitude cyclone and its associated thermal advection pattern entered the TC environment. Consequently, the decaying TC either remains a secondary circulation that moves around the primary midlatitude cyclone, which occurred with TY Opal, or undergoes a period of weak development until the system reaches a more favorable upper-tropospheric environment for development.

TABLE 3. Kinetic energy budget as in Table 1, except for TY Opal.

Date	K	$\partial K/\partial t$	HFC	GKE	$D(k)$
0000 UTC 20 Jun 97	3.7	1.7	−2.0	6.9	3.2
1200 UTC 20 Jun 97	5.3	1.9	−1.2	3.6	0.5
0000 UTC 21 Jun 97	5.4	0.7	−2.3	8.0	5.0
1200 UTC 21 Jun 97	5.8	0.7	0.23	7.6	7.1

The kinetic energy budget clarifies the effects of coupling between the TC and the midlatitude circulation pattern. As the TC moves into the midlatitudes, energy is exported from the region as the upper-level TC outflow crossing toward lower pressure heights in the trough acts to also accelerate the winds downstream from the TC. The horizontal loss of energy may be compensated by a generation of kinetic energy associated with baroclinic or barotropic conversions. During the northwest ET, convergent flow contributed to generation of kinetic energy at low levels with an expansion of the cyclonic circulation during reintensification (Fig. 7). The coupling between the TC and midlatitude trough to the northwest contributes to the eddy heat fluxes and conversion of available potential energy into kinetic energy via solenoidal circulations in which cold air sinks to the west of David and warm air rises to the east of David. At upper levels, two-thirds of the generation of kinetic energy due to flow toward lower heights was associated with the acceleration of nondivergent winds downstream of the TC, and one-third was contributed by divergent flow toward lower heights due to the velocity potential maximum above the decaying TC.

The transition of Opal into a northeast pattern also included an upper-level kinetic energy export due to the

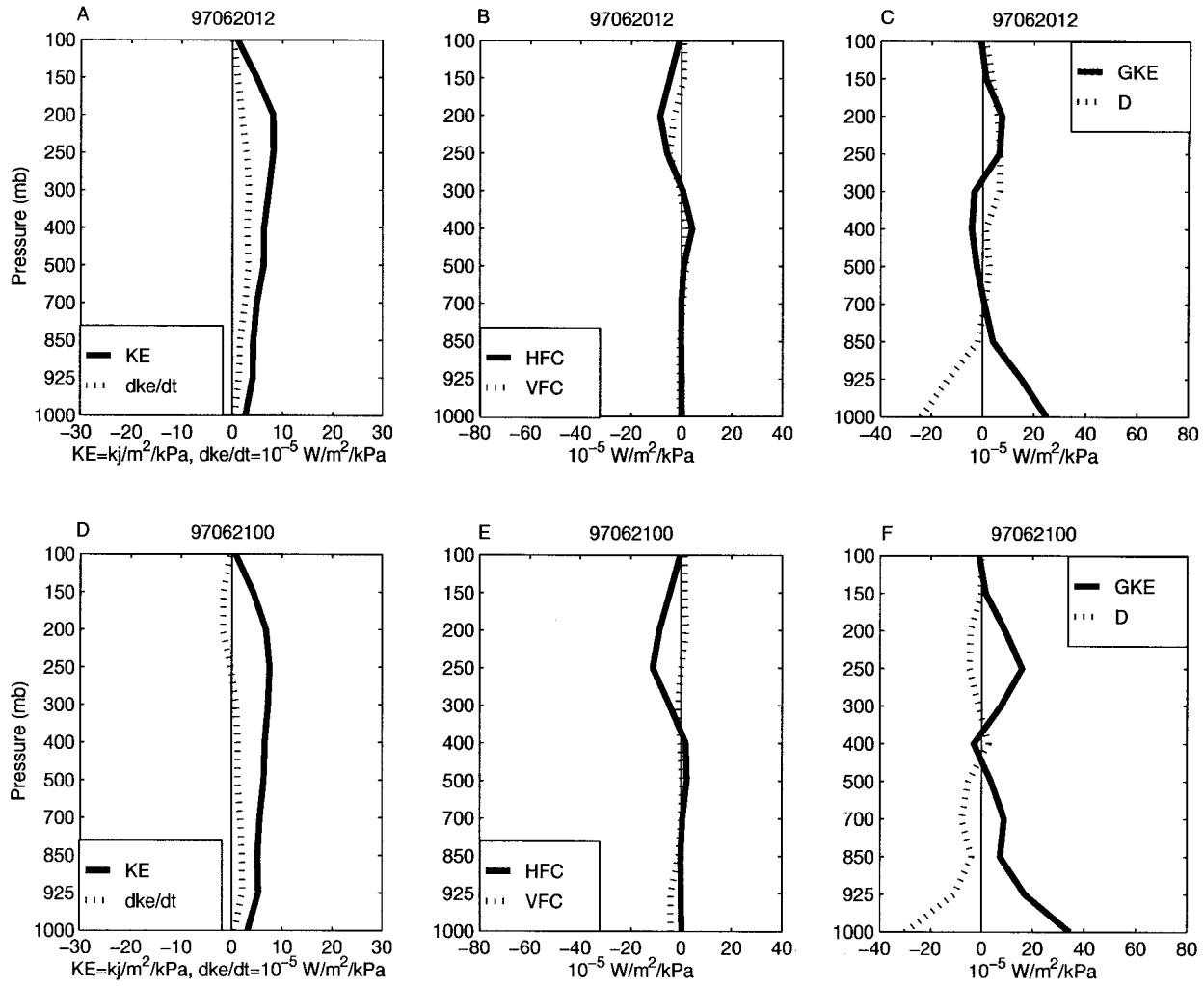

FIG. 16. Vertical distributions of the terms in the kinetic energy budget equation as in Fig. 12 for TY Opal at the times indicated above each panel. Kinetic energy is in units of kJ m^{-2} kPa^{-1} and changes in kinetic energy are in 10^{-5} W m^{-2} kPa^{-1}.

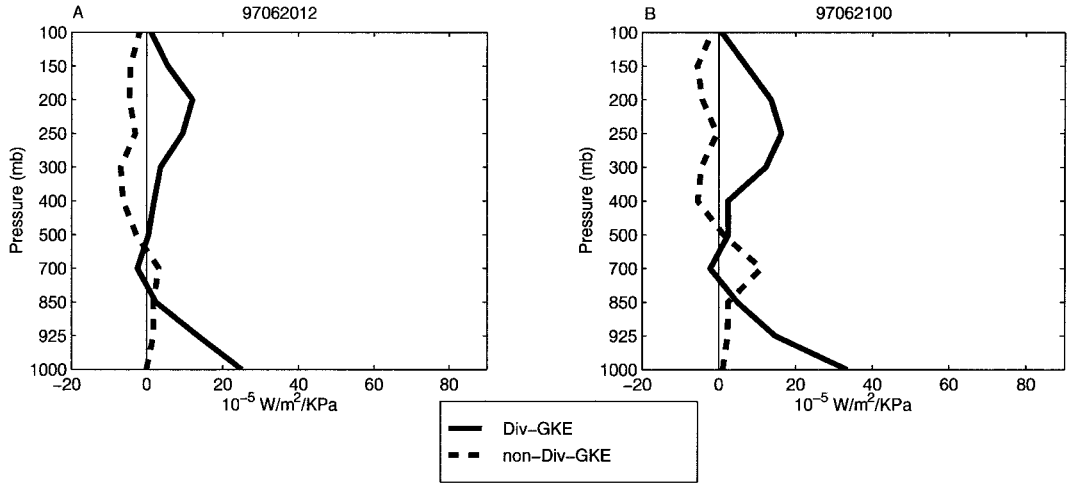

FIG. 17. Vertical distribution of the generation of kinetic energy (10^{-5} W m^{-2} kPa^{-1}) due to the divergent (solid lines) and nondivergent (dashed lines) winds as in Fig. 14, except for TY Opal at the times indicated above each panel.

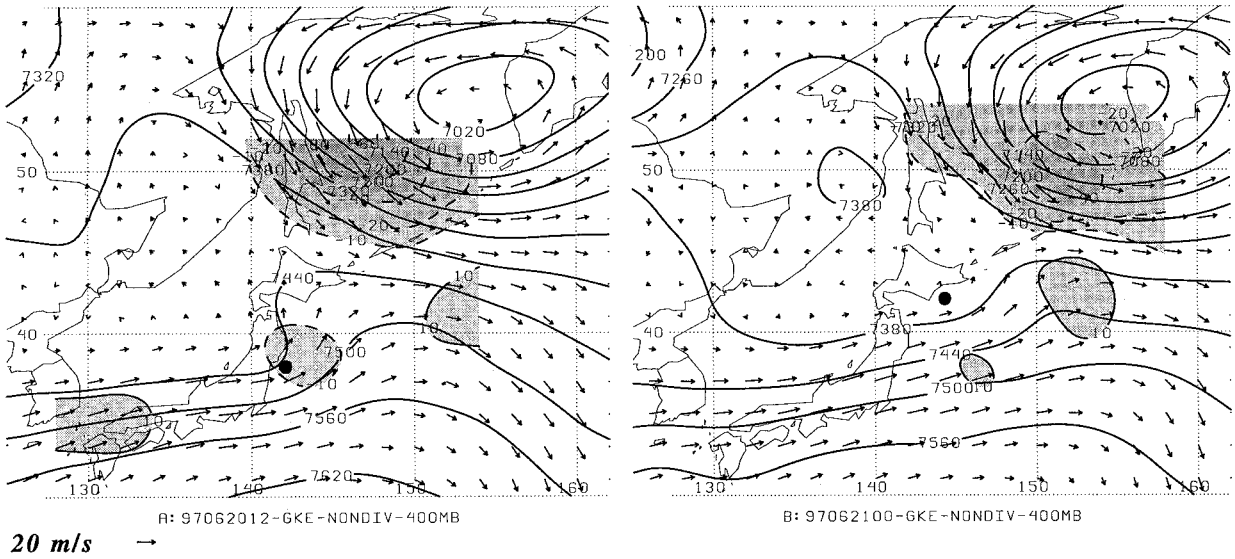

FIG. 18. Analyzed heights (m, solid contours) at 400 hPa, winds (m s^{-1} arrows, scale at bottom left), and generation of kinetic energy (10^{-5} W m^{-2} kPa^{-1} shaded, negative contours are dashed) for (a) 1200 UTC 20 Jun and (b) 0000 UTC 21 Jun. The black circle in each panel marks the low-level center of Opal.

acceleration of winds downstream from the TC. However, the upper-level energy source due to the nondivergent winds, which was the primary energy source in David, contributed to the destruction of kinetic energy during the ET of Opal. This destruction was due to the deceleration and turning to higher heights where the flow around the midlatitude cyclone to the northeast approached Opal.

Although the ET of a TC involves many complex physical mechanisms, the goal of this study and of Harr and Elsberry (2000) has been to address the impact of different midlatitude circulation patterns on ET over the western North Pacific. Many characteristics during the transformation stage of ET as defined by Klein et al. (2000) may be attributed to the initial movement of a TC into the midlatitude environment. Also, the initial formation of frontal regions defined by Harr and Elsberry (2000) was attributed to the kinematics associated with the movement of the TC into the midlatitude westerlies. However, these analyses, and those in Harr and Elsberry (2000), indicate that the *final* result of ET, which is a mature extratropical cyclone, depends on the character of the circulation pattern into which the TC moves. In a northeast circulation pattern, the TC cir-

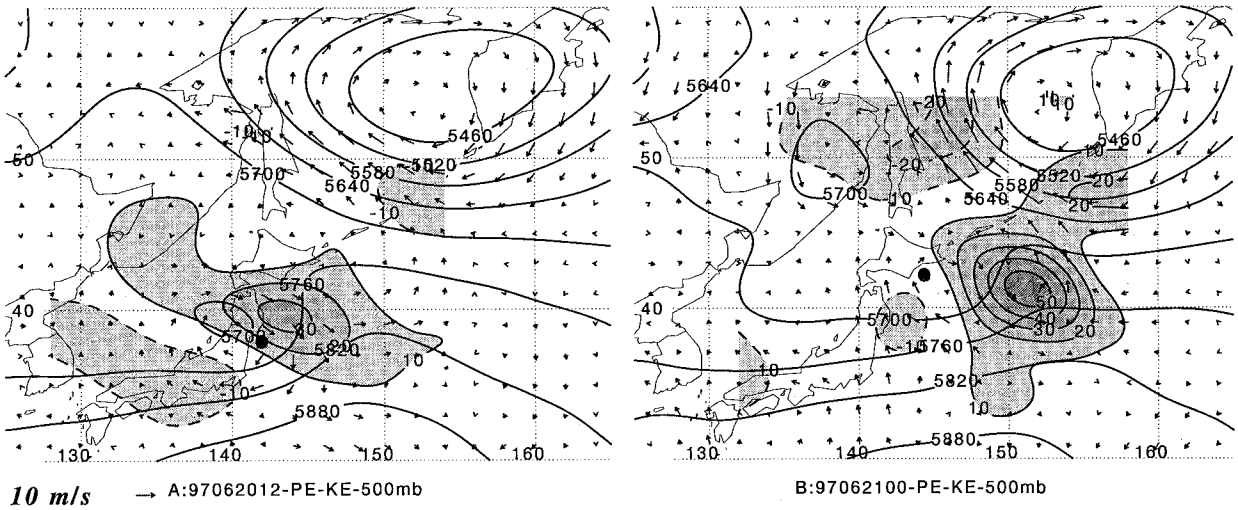

FIG. 19. Analyzed heights (m, solid contours) at 250 hPa, ageostrophic winds (m s^{-1} arrows, scale at bottom left), and conversion of available potential energy into kinetic energy (10^{-5} W m^{-2} kPa^{-1} shaded, negative contours are dashed) for (a) 1200 UTC 20 Jun and (b) 0000 UTC 21 Jun. The black circle in each panel marks the low-level center of Opal.

TABLE 4. The HFC and GKE contributions to kinetic energy as in Table 2, except for TY Opal.

Date	HFC	HFC_r	HFC_d	GKE	GKE_r	GKE_d
0000 UTC 20 Jun 97	−2.0	−2.0	−0.002	6.9	1.9	5.0
1200 UTC 20 Jun 97	−1.2	−2.1	0.9	3.6	−2.1	5.7
0000 UTC 21 Jun 97	−2.3	−2.9	0.6	8.0	−0.4	8.4
1200 UTC 21 Jun 97	0.23	−1.3	1.5	7.6	0.0	7.6

culation is prevented for at least 36 h from coupling with the midlatitude baroclinic zone in such a manner that would allow significant reintensification. Whereas in the northwest pattern coupling between the TC and midlatitude circulations occurs in conjunction with the initial movement of the TC into the midlatitude westerlies.

Some of the differences in extratropical cyclone paths and short-term (<36 h) reintensification may be attributed to how the decaying TC interacts with either the northwest or northeast midlatitude circulation. However, variabilities in TC characteristics such as size and intensity need to be addressed in more detail. The reintensification of the extratropical cyclone may also be impacted by other factors such as static stability and surface fluxes over a warm or a cold ocean, which were not considered in this study of the impact of the synoptic-scale influences. Finally, the relationship between forecast accuracy and each type of ET needs to be examined.

Acknowledgments. This research was sponsored by the Office of Naval Research Marine Meteorology Program and the Atmospheric Directorate of the Naval Research Laboratory. Discussions with Prof. John Molinari concerning the application of the EP flux calculations are gratefully acknowledged. The NOGAPS fields were processed at the High Performance Computing Center, Stennis Space Center, Mississippi.

REFERENCES

Andrews, D. G., 1983: A finite-amplitude Eliassen-Palm theorem in isentropic coordinates. *J. Atmos. Sci.*, **40,** 1877–1883.

Anthes, R. A., 1990: Advances in the understanding and prediction of cyclone development with limited-area fine-mesh models. *Extratropical Cyclones: The Erik Palmen Memorial Volume*, C. W. Newton and E. O. Holopainen, Eds., Amer. Meteor. Soc., Boston, 221–254.

Bosart, L. F., and G. M. Lackmann, 1995: Postlandfall tropical cyclone reintensification in a weakly baroclinic environment: A case study of hurricane David (September 1979). *Mon. Wea. Rev.*, **123,** 3268–3291.

Browning, K. A., G. Vaughan, and P. Panagi, 1998: Analysis of an ex-tropical cyclone after its reintensification as a warm-core extratropical cyclone. *Quart. J. Roy. Meteor. Soc.*, **124,** 2329–2356.

Chen, T.-C., J. C. Alpert, and T. W. Schlatter, 1978: The effects of divergent and nondivergent winds on the kinetic energy budget of a mid-latitude cyclone: A case study. *Mon. Wea. Rev.*, **106,** 458–468.

Chien, H. H., and P. J. Smith, 1977: Synoptic and kinetic energy analyses of Hurricane Camille (1969) during transit across the southeastern United States. *Mon. Wea. Rev.*, **105,** 67–77.

Davies, H. C., C. Schar, and H. Wernli, 1991: The palette of fronts and cyclones within a baroclinic wave development. *J. Atmos. Sci.*, **48,** 1666–1689.

DiMego, G. J., and L. F. Bosart, 1982a: The transformation of tropical storm Agnes into an extratropical cyclone. Part I: The observed fields and vertical motion computations. *Mon. Wea. Rev.*, **110,** 385–411.

——, and ——, 1982b: The transformation of tropical storm Agnes into an extratropical cyclone. Part II: Moisture, vorticity and kinetic energy budgets. *Mon. Wea. Rev.*, **110,** 412–433.

Edmon, H. J., B. J. Hoskins, and M. E. McIntyre, 1980: Eliassen-Palm cross sections for the troposphere. *J. Atmos. Sci.*, **37,** 2600–2616; Corrigendum, **38,** 1115.

Eliassen, A., and E. Palm, 1961: On the transfer of energy in stationary mountain waves. *Geofys. Publ.*, **22** (3), 1–23.

Evans, M. S., D. Keyser, L. F. Bosart, and G. M. Lackmann, 1994: A satellite-derived classification scheme for rapid maritime cyclogenesis. *Mon. Wea. Rev.*, **122,** 1381–1416.

Harr, P. A., and R. L. Elsberry, 2000: Extratropical transition of tropical cyclones over the western North Pacific. Part I: Evolution of structural characteristics during the transition process. *Mon. Wea. Rev.*, **128,** 2613–2633.

Hirschberg, P. A., and J. M. Fritsch, 1991a: Tropopause undulations and the development of extratropical cyclones. Part I: Overview and observations from a cyclone event. *Mon. Wea. Rev.*, **119,** 496–517.

——, and ——, 1991b: Tropopause undulations and the development of extratropical cyclones. Part II: Diagnostic analysis and conceptual model. *Mon. Wea. Rev.*, **119,** 518–550.

Hogan, T. F., and T. E. Rosmond, 1991: The description of the Navy Operational Global Atmospheric Prediction System's spectral forecast model. *Mon. Wea. Rev.*, **119,** 1786–1815.

Klein, P. M., P. A. Harr, and R. L. Elsberry, 2000: Extratropical transition of western North Pacific tropical cyclones: An overview and conceptual model of the transformation stage. *Wea. Forecasting*, **15.** 373–395.

Kornegay, F. C., and D. G. Vincent, 1976: Kinetic energy budget analysis during interaction of tropical storm Candy (1968) with and extratropical frontal system. *Mon. Wea. Rev.*, **104,** 849–859.

Molinari, J., and D. Vollaro, 1989: External influences on hurricane intensity. Part I: Outflow-layer eddy angular momentum fluxes. *J. Atmos. Sci.*, **46,** 1093–1105.

——, and ——, 1990: External influences on hurricane intensity. Part II: Vertical structure and response of the hurricane vortex. *J. Atmos. Sci.*, **47,** 1902–1918.

——, S. Skubis, and D. Vollaro, 1995: External influences on hurricane intensity. Part III: Potential vorticity structure. *J. Atmos Sci.*, **52,** 3593–3606.

——, ——, ——, F. Alsheimer, and H. E. Willoughby, 1998: Potential vorticity analysis of tropical cyclone intensification. *J. Atmos. Sci.*, **55,** 2632–2644.

Newton, C. W., 1990: Erik Palmen's contributions to the development of cyclone concepts. *Extratropical Cyclones, The Erik Palmen Memorial Volume*, C. W. Newton and E. O. Holopainen, Eds., Amer. Meteor. Soc., 1–18.

Palmen, E., 1958: Vertical circulation and release of kinetic energy during the development of hurricane Hazel into an extratropical cyclone. *Tellus*, **10,** 1–23.

Richman, M. B., 1986: Rotation of principal components. *Int. J. Climatol.*, **6,** 293–335.

Sinclair, M. R., 1993: Synoptic-scale diagnosis of the extratropical transition of a southwest Pacific tropical cyclone. *Mon. Wea. Rev.*, **121,** 941–960.

——, and M. J. Revell, 2000: Classification and composite diagnosis of extratropical cyclogenesis events in the southwest Pacific. *Mon. Wea. Rev.*, **128,** 1089–1105.

Schultz, D. M., D. Keyser, and L. F. Bosart, 1998: The effect of large-

scale flow on low-level frontal structure and evolution in mid-latitude cyclones. *Mon. Wea. Rev.*, **126,** 1767–1791.
Thorncroft, C. D., B. J. Hoskins, and M. E. McIntyre, 1993: Two paradigms of baroclinic-wave life-cycle behavior. *Quart. J. Roy. Meteor. Soc.*, **119,** 17–55.
Vincent, D. G., and L. N. Chang, 1975: Kinetic energy budgets of moving systems: Case studies for an extratropical cyclone and Hurricane Celia. *Tellus*, **27,** 215–233.
Whitaker, J. S., and A. Barcilon, 1992: Type B cyclogenesis in a zonally varying flow. *J. Atmos. Sci.*, **49,** 1877–1892.